Fracture Mechanisms in Bulk Metallic Glassy Materials

Z. F. Zhang,[1,2,*] G. He,[1] J. Eckert,[1] and L. Schultz[1]

[1]*IFW Dresden, Institute of Metallic Materials, 01069 Dresden, Germany*
[2]*Shenyang National Laboratory for Materials Science, Institute of Metal Research, Chinese Academy of Sciences,*
110016 Shenyang, People's Republic of China

We find that the failure of bulk metallic glassy (BMG) materials follows three modes, i.e., shear fracture with a fracture plane significantly deviating from 45° to the loading direction, normal tensile fracture with a fracture plane perpendicular to the loading direction, or distensile fracture in a break or splitting mode with a fracture plane parallel to the loading direction. The actually occurring type of failure strongly depends on the applied loading mode and the microstructure of the material. Extensive evidence indicates that the Tresca fracture criterion is invalid, and for the first time, three fracture criteria are developed for isotropic materials with high strength, such as advanced BMGs or the newly developed bulk nanostructural materials.

Bulk metallic glass (BMG) materials possess remarkable physical, chemical, and mechanical properties and have potential applications in many areas, which have created extensive interest among scientists and engineers [1,2]. Normally, metallic glasses often deform by the formation of localized shear bands and display little plasticity before fracture at room temperature [3–6]. However, abundant observations [7–20] show that BMGs always fracture along a plane deviating from the maximum shear stress plane, which is not in agreement with the Tresca criterion [19]. On the other hand, recently developed BMG composites containing nanocrystals, hard particles, strong fibers, or ductile phases can exhibit high strength and good ductility [21–27]. However, multifarious fracture behavior is frequently observed [24–27] and can be attributed to the special nature of the BMG materials. The present research will elucidate all the possible fracture phenomena of BMGs induced by uniaxial loading. Based on our experiments, we have developed comprehensive criteria to explain the various existing fracture mechanisms, which can be widely used for isotropic materials with high strength.

The Tresca criterion [19] considers that fracture always occurs along the maximum shear stress plane at a critical shear stress τ_0. Therefore, all metallic glassy specimens should preferentially fracture along the maximum shear stress plane (45°) no matter whether under tension or compression. However, extensive investigations from the 1970s to present show that the fracture angles between the stress axis and the shear plane of metallic glasses always deviate from 45°, as listed in Table I [7–20]. Our recent investigations also reveal such a shear fracture behavior for different BMGs under tension and compression. The typical shear fracture behavior of BMGs is illustrated in Figs. 1(a)–1(c). For $Zr_{59}Cu_{20}Al_{10}Ni_8Ti_3$, $Zr_{54.5}Cu_{20}Al_{10}Ni_8Ti_{7.5}$, $Zr_{55}Cu_{30}Al_{10}Ni_5$, and $Zr_{52.5}Cu_{17.9}Al_{10}Ni_{14.6}Ti_5$ metallic glasses, the compressive fracture angle θ_C between the compressive axis

and the fracture plane is in the range of 40°–43°. For some BMG composites containing Ta particles or dendritic precipitates $[(Zr_{0.55}Cu_{0.30}Al_{0.10}Ni_{0.05})_{95}Ta_5$ or $Ti_{56}Cu_{16.8}Ni_{14.4}Sn_{4.8}Nb_8]$, their θ_C is only about 32° or 27°, respectively, revealing an even more significant deviation from 45°. Obviously, Ta particles or dendritic precipitates greatly change the shear fracture plane of the BMG composites. Moreover, we also found that the tensile fracture angles θ_T of $Zr_{59}Cu_{20}Al_{10}Ni_8Ti_3$ and $Zr_{52.5}Cu_{17.9}Al_{10}Ni_{14.6}Ti_5$ metallic glasses are equal to 54° and 56°, respectively. This agrees well with previous findings, i.e., θ_T approximately deviates 5°–20° from 45° for different BMG materials. Based on the data available (Table I) and the present results, it can be concluded that the shear fracture of metallic glasses does not obey the Tresca criterion [19], namely, θ_T is larger than 45°, but θ_C is smaller than 45°:

$$0 < \theta_C < 45° < \theta_T < 90°. \tag{1}$$

Accordingly, there must exist a shear fracture mechanism different from the Tresca criterion. Since all the BMG materials possess very high strength (1.5–2.5 GPa), the normal stress applied on the shear plane is also very high (~ 1 GPa) and must play an important role in the fracture process. Under tension or compression, the stress state ($\sigma_\theta, \tau_\theta$) of a specimen on any plane can be illustrated as in Fig. 1(d). If the normal stress (σ_C or σ_T) on the shear plane is taken into account, similar to the Mohr-Coulomb model [19], we can express the critical fracture stress (τ_C or τ_T) for both shear compressive and tensile failure as

$$\tau_C = \tau_0 + \mu_C\sigma_C \quad \text{(for compression)}, \tag{2a}$$
$$\tau_T = \tau_0 - \mu_T\sigma_T \quad \text{(for tension)}. \tag{2b}$$

Here μ_C and μ_T are two constants for compression and tension and will be discussed later.

TABLE I. Compressive and tensile fracture angles θ_C and θ_T for different BMG materials.

	Investigators	Composites	θ_C
	He et al. [10]	$Zr_{52.5}Ni_{14.6}Al_{10}Cu_{17.9}Ti_5$	$40°-45°$
	Lowhaphandu et al. [14]	$Zr_{62}Ti_{10}Ni_{10}Cu_{14.5}Be_{3.5}$	$41.6° \pm 2.1°$
	Donovan [19]	$Pd_{40}Ni_{40}P_{20}$	$41.9° \pm 1.2°$
	Wright et al. [20]	$Zr_{40}Ti_{14}Ni_{10}Cu_{12}Be_{24}$	$42°$
	Present results (I)	$Zr_{59}Cu_{20}Al_{10}Ni_8Ti_3$	$43°$
Compressive Fracture		$Zr_{55}Cu_{30}Al_{10}Ni_5$	$40°-43°$
		$Zr_{54.5}Cu_{20}Al_{10}Ni_8Ti_{7.5}$	$42°$
		$Zr_{52.5}Ni_{14.6}Al_{10}Cu_{17.9}Ti_5$	$42°$
		$(Zr_{55}Cu_{30}Al_{10}Ni_5)_{1-0.95}Ta_5$	$31°-33°$
		$Ti_{56}Cu_{16.8}Ni_{14.4}Sn_{4.8}Nb_8$	$27°$
		$Ti_{56}Cu_{16.8}Ni_{14.4}Sn_{4.8}Nb_8$	Split ($\approx 0°$)
		$Zr_{55}Cu_{30}Al_{10}Ni_5$[a]	Break or split
		$Ti_{50}Cu_{20}Ni_{23}Sn_7$	Break or split

	Investigators	Composites	θ_T
	Alpas et al. [7]	$Ni_{78}Si_{10}B_{12}$	$55°$
	Bengus et al. [8]	$Fe_{70}Ni_{10}B_{20}$	$60°$
	Davis and Yeow [9]	$Ni_{49}Fe_{29}P_{14}B_6Si_2$	$53°$
	He et al. [10]	$Zr_{52.5}Ni_{14.6}Al_{10}Cu_{17.9}Ti_5$	$55°-65°$
	Inoue et al. [11]	$Zr_{65}Ni_{10}Al_{7.5}Cu_{7.5}Pd_{10}$	$50°$
	Inoue et al. [12]	$Cu_{60}Zr_{30}Ti_{10}$	$54°$
Tensile Fracture	Liu et al. [13]	$Zr_{52.5}Ni_{14.6}Al_{10}Cu_{17.9}Ti_5$	$53°-60°$
	Lowhaphandu et al. [14]	$Zr_{62}Ti_{10}Ni_{10}Cu_{14.5}Be_{3.5}$	$57° \pm 3.7°$
	Megusar et al. [15]	$Pd_{80}Si_{20}$	$50°$
	Mukai et al. [16]	$Pd_{40}Ni_{40}P_{20}$	$56°$
	Noskova et al. [17]	$Co_{70}Si_{15}B_{10}Fe_5$	$60°$
	Takayama [18]	$Pd_{77.5}Cu_6Si_{16.5}$	$50°-51°$
	Present results (II)	$Zr_{52.5}Ni_{14.6}Al_{10}Cu_{17.9}Ti_5$	$56°$
		$Zr_{59}Cu_{20}Al_{10}Ni_8Ti_3$	$54°$
		$Zr_{52.5}Ni_{14.6}Al_{10}Cu_{17.9}Ti_5$[a]	$\approx 90°$
		$Zr_{59}Cu_{20}Al_{10}Ni_8Ti_3$[a]	$\approx 90°$

[a]The three metallic glassy materials were annealed at 420 °C for 5, 10, and 20 min for partial or full crystallization.

In a $\sigma - \tau$ coordinate, Eqs. (2a) and (2b) can be plotted in Fig. 1(e), where μ_T and μ_C are equal to the slopes of the critical tensile and compressive fracture lines AB and AE, respectively. Meanwhile, another constant σ_0 can be regarded as the critical normal fracture stress under the condition without shear stress and $\mu_T = \tau_0/\sigma_0$. Under tension or compression, the stress state $(\sigma_\theta, \tau_\theta)$ on any shear plane will distribute on the Mohr circles **a** or **b** in Fig. 1(e). When the Mohr circles touch the critical fracture lines AB or AE, the tangency points $C(\sigma_\theta, \tau_\theta)$ or $D(\sigma_\theta, \tau_\theta)$ correspond to the critical shear fracture stress state of the specimen. Therefore, the diameters of the two Mohr circles represent tensile or compressive shear fracture strength (σ_F^T or σ_F^C) and can be deduced as

$$\sigma_F^T = \frac{2\tau_0}{\sqrt{1 + (\mu_T)^2} + \mu_T}, \quad (3a)$$

$$\sigma_F^C = \frac{2\tau_0}{\sqrt{1 + (\mu_C)^2} - \mu_C}. \quad (3b)$$

From Fig. 1(e), tensile and compressive shear fracture angles θ_T and θ_C can be expressed as

$$\theta_T = \arctan(\sqrt{1 + (\mu_T)^2} + \mu_T) > 45°, \quad (4a)$$

$$\theta_C = \arctan(\sqrt{1 + (\mu_C)^2} - \mu_C) < 45°. \quad (4b)$$

Therefore, the shear fracture strengths (σ_F^T or σ_F^C) and shear fracture angles (θ_T and θ_C) are functions of τ_0, μ_C, and μ_T ($= \tau_0/\sigma_0$). From Eqs. (4a) and (4b) or Fig. 1(e), it is apparent that θ_T is larger than 45°, as given by Eq. (1). This explains why the shear fracture of most BMG materials does not occur at the maximum shear stress plane [7–20].

Fractography observations showed that the typical compressive shear fracture surface exhibits only a vein-like structure with a rather uniform arrangement, showing a pure shear fracture mode [Fig. 2(a)]. This vein structure has been widely observed before and was attributed to melting of metallic glasses [12–16,20]. However, on the tensile fracture surfaces, two typical features, i.e., some round cores and radiating veins, are observed for the first time, as shown in Fig. 2(b). We consider that (i) the veins originate from the cores and propagate
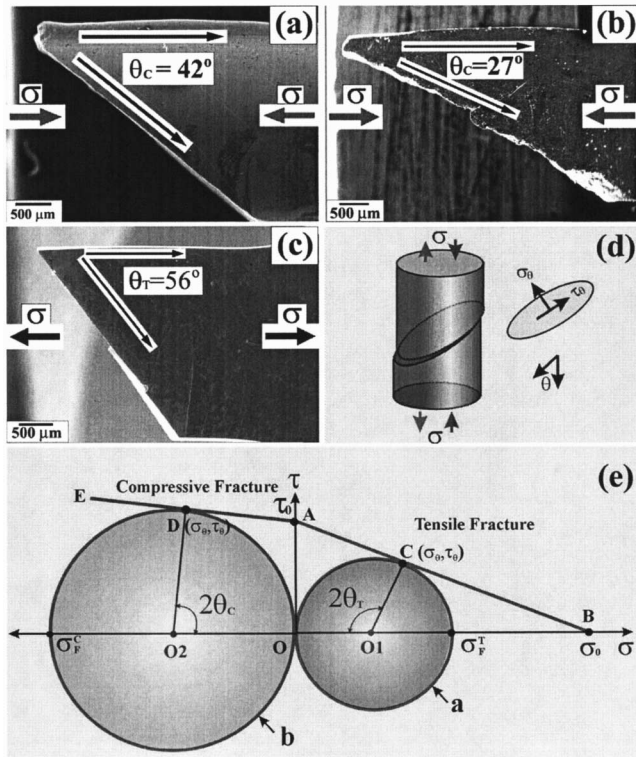
FIG. 1. Typical shear fracture modes of BMG materials under tension and compression. Compressive shear fracture of (a) $Zr_{55}Cu_{30}Al_{10}Ni_5$ metallic glass and (b) $Ti_{56}Cu_{16.8}Ni_{14.4}Sn_{4.8}Nb_8$ composite containing dendritic precipitates; (c) tensile shear fracture of $Zr_{52.5}Ni_{14.6}Al_{10}Cu_{17.9}Ti_5$ metallic glass; (d) illustration of shear and normal stresses on any plane of a specimen under compression or tension; (e) schematic illustration of the critical tensile and compressive fracture lines (AB and AE) and the stress distribution on the two Mohr circles under tension and compression.

towards the outside in a radial mode; (ii) tensile fracture does not occur in a pure shear mode and is distinctly different from the compressive fracture feature. These observations further provide powerful evidence for the significant difference in the fracture features of BMGs induced by compression and tension. Therefore, both the macroscopic stress state and the micrometer-scale fracture feature of BMGs support the deviation of θ_T and θ_C from the maximum shear stress plane due to a restraining effect under normal compressive stress or a promotion effect under normal tensile stress.
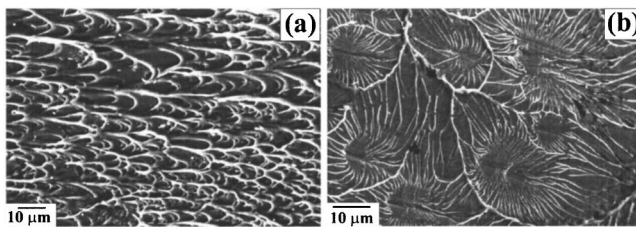

FIG. 2. Typical shear fracture surface features of metallic glasses under (a) compression and (b) tension.

Besides the shear fracture, there are some other fracture modes for BMG materials. For example, annealed $Zr_{59}Cu_{20}Al_{10}Ni_8Ti_3$ and $Zr_{52.5}Cu_{17.9}Al_{10}Ni_{14.6}Ti_5$, which contain a high volume fraction of nanocrystals ($V_f >$ 50%), always show nearly zero tensile fracture strength and their fracture surfaces are approximately perpendicular to the loading axis [Fig. 3(a)]. Another typical failure mode is that the specimens often break into many small pieces rather than fracture in a shear mode, when the partially or fully crystallized metallic glass (for example, $Zr_{55}Cu_{30}Al_{10}Ni_5$) is subjected to compressive loading. In some cases, BMG composites containing dendritic phases ($Ti_{50}Cu_{23}Ni_{20}Sn_7$ or $Ti_{56}Cu_{16.8}Ni_{14.4}Sn_{4.8}Ta_8$) split into several parts [Fig. 3(b)] or fracture along a plane nearly parallel to the compressive axis [Fig. 3(c)], which is different from the wing cracks proposed by Ashby et al. [28]. A similar fracture phenomenon, such as buckling and consequent delamination, also occurs in other BMG composites [24–27]. This indicates that BMG composites with nanocrystals, hard particles, strong fibers, or dendritic phases do not always fracture in a shear mode. Here, we define the two observed failure modes as normal tensile fracture (TF) with a fracture plane perpendicular to the loading direction and distensile fracture (DF) in a break or splitting mode with a fracture plane parallel to the loading direction, respectively.

Normal TF of the crystallized metallic glasses always occurs at very low tensile fracture strength and can be schematically illustrated as in Fig. 3(d). The tensile stress Mohr circle **a** is very small and the tensile strength σ_T is approximately equal to σ_0. Therefore, the critical tensile fracture line AB is nearly perpendicular to the normal
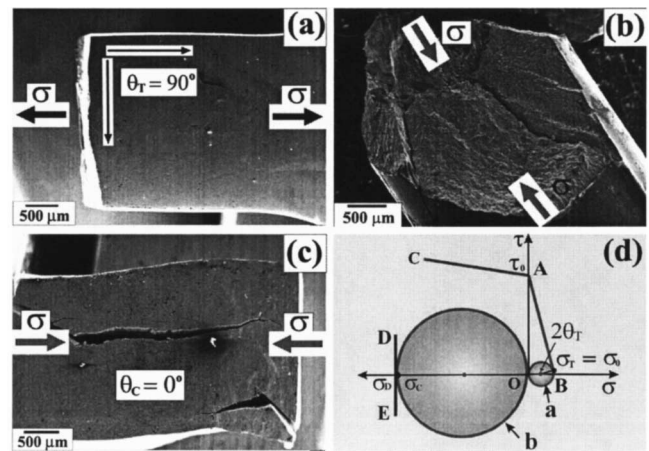

FIG. 3. (a) Normal tensile fracture of the crystallized $Zr_{59}Cu_{20}Al_{10}Ni_8Ti_3$ metallic glass containing brittle Zr_2Cu nanocrystals. (b) Fracture of $Ti_{50}Cu_{20}Ni_{23}Sn_7$ metallic glassy composite containing dendritic precipitates under compression. (c) Split of $Ti_{56}Cu_{16.8}Ni_{14.4}Sn_{4.8}Ta_8$ metallic glassy composite containing dendritic precipitates under compression. (d) Variation of the critical compressive and tensile fracture conditions due to the change in the microstructure of the BMG materials.

stress axis σ and θ_T is quite close to 90°. From Eq. (4a), when $\mu_T \rightarrow \infty$, normal tensile fracture will occur at an angle θ_T close to 90°. The great increase of $\mu_T = \tau_0/\sigma_0 \rightarrow \infty$ can be attributed to the extremely low value of σ_0 due to the crystallization treatment, which results in the formation of nanocrystals, such as brittle intermetallic compounds [10,11].

The DF mechanism is difficult to understand and was never explained before. As shown in Fig. 3(d) and Table I, since the compressive specimens break or split into two or several parts, here we define a critical distensile fracture stress σ_D as shown in Fig. 3(d). When σ_D is smaller than the critical shear fracture stress σ_F^C, i.e.,

$$\sigma_D < \sigma_F^C = \frac{2\tau_0}{\sqrt{1 + (\mu_C)^2} - \mu_C}, \qquad (5)$$

the stress Mohr circle **b** in Fig. 3(d) will first touch the distensile fracture line DE. In this case, the specimen will fracture in a distensile mode first rather than in a shear mode, due to local cracking rather than macroscopic shear cracking of the composite. On the contrary, when σ_D is higher than σ_F^C, the specimen will still fracture a shear mode.

Therefore, the fracture plane of BMGs can make any angle from 0° to 90° with respect to the stress axis. The actual failure of a BMG material is a competitive process between shear, distensile, and normal tensile fracture, depending on the loading mode and the inhomogeneity of the microstructure. Normal tensile and distensile fracture can be regarded as two special cases of shear fracture. The multifarious fracture mechanisms can be attributed to either an inhomogeneous distribution of the strengthening phases in the composites or the weak bonding of the interfaces between the matrix and the strengthening phases. Since the strengthening phases can also change the shear fracture angles θ_C and θ_T of the BMG materials, the physical meaning of the two constants μ_C and μ_T must reflect the degree of homogeneity in the microstructure of BMG materials. The occurrence of distensile fracture or not depends on the values of μ_C and μ_T and is a result of the interactions between the strengthening phases and the matrix of the composites [21–27], which are substantially important for further optimizing the properties of the BMG composites through the control of the microstructure.

With the development of advanced materials, new fracture features are of interest in the mechanics and physics of the materials. BMGs and their composites, as typical super-high-strength materials, display abnormal fracture behavior in comparison with traditional crystalline materials. The finding of the new fracture modes of BMG materials and their fracture criteria will contribute to the optimum design and fabrication of new high-performance materials. For example, recently, we successfully fabricated novel BMG materials with high strength and good ductility through the control of composition and microstructure [27]. We suggest that the present fracture criteria can be widely employed for isotropic materials with high strength, such as advanced BMGs or the newly developed bulk nanostructural materials.

*Corresponding author.
  Present address: Max-Planck-Institut für Metallforchung, Heisenbergstrasse 3, 70569 Stuttgart, Germany.

[1] W. L. Johnson, MRS Bull. **24**, 42–56 (1999).
[2] A. Inoue, Acta Mater. **48**, 279–306 (2000).
[3] C. A. Pampillo, J. Mater. Sci. **10**, 1194–1227 (1975).
[4] F. Spaepen, Acta Metall. **25**, 407–415 (1977).
[5] A. S. Argon, Acta Metall. **27**, 47–58 (1979).
[6] H. Chen, Y. He, G. J. Shiflet, and S. J. Poon, Nature (London) **367**, 541–543 (1994).
[7] A. T. Alpas, L. Edwards, and C. N. Reid, Metall. Trans. A **20**, 1395–1409 (1989).
[8] V. Z. Bengus et al., J. Mater. Sci. **25**, 1598–1602 (1990).
[9] L. A. Davis and Y. T. Yeow, J. Mater. Sci. **15**, 230–236 (1980).
[10] G. He et al., Mater. Trans. **42**, 356–364 (2001).
[11] A. Inoue, H. M. Kimura, and T. Zhang, Mater. Sci. Eng., A **294–296**, 727–735 (2000).
[12] A. Inoue, W. Zhang, T. Zhang, and K. Kurosaka, Acta Mater. **49**, 2645–2652 (2001).
[13] C. T. Liu et al., Metall. Mater. Trans. A **29**, 1811–1820 (1998).
[14] P. Lowhaphandu, L. A. Ludrosky, S. L. Montgomery, and J. J. Lewandowski, Intermetallics **8**, 487–492 (2000).
[15] J. Megusar, A. S. Argon, and N. J. Grant, Mater. Sci. Eng. **38**, 63–72 (1979).
[16] T. Mukai et al., Scr. Mater. **46**, 43–47 (2002).
[17] N. I. Noskova, N. F. Vildanova, Y. I. Filippov, and A. P. Potapov, Phys. Status Solidi A **87**, 549–557 (1985).
[18] S. Takayama, Scr. Metall. **13**, 463–467 (1979).
[19] P. E. Donovan, Acta Metall. **37**, 445–456 (1989).
[20] W. J. Wright, R. Saha, and W. D. Nix, Mater. Trans. **42**, 642–649 (2001).
[21] C. C. Hays, C. P. Kim, and W. L. Johnson, Phys. Rev. Lett. **84**, 2901–2904 (2000).
[22] L. Q. Xing et al., Phys. Rev. B **64**, R180201 (2001).
[23] C. Fan, R. T. Ott, and T. C. Hufnagel, Appl. Phys. Lett. **81**, 1020–1022 (2002).
[24] R. D. Conner, R. B. Dandliker, and W. L. Johnson, Acta Mater. **46**, 6089–6102 (1998).
[25] F. Szuecs, C. P. Kim, and W. L. Johnson, Acta Mater. **49**, 1507–1513 (2001).
[26] G. He, W. Löser, J. Eckert, and L. Schultz, J. Mater. Res. **17**, 3015–3018 (2002).
[27] G. He, W. Löser, J. Eckert, and L. Schultz, Nature Mater. **2**, 33–37 (2003).
[28] M. F. Ashby and S. D. Hallam, Acta Metall. **34**, 497–510 (1986).